J Mater Sci (2020) 55:15709–15725

Composites & nanocomposites

Rheological behavior, 3D printability and the formation of scaffolds with cellulose nanocrystals/gelatin hydrogels

Yani Jiang[1], Jiping Zhou[1,*], Cheng Feng[3], Hongcan Shi[2], Guoqi Zhao[3], and Yixiang Bian[1]

[1] College of Mechanical Engineering, Yangzhou University, No. 196 West Huayang Road, Yangzhou, China
[2] Medical College of Yangzhou University, No. 11 Huaihai Road, Yangzhou, China
[3] College of Animal Science and Technology, Yangzhou University, No. 48 East Wenhui Road, Yangzhou, China

Received: 29 April 2020
Accepted: 18 July 2020
Published online: 26 August 2020

ABSTRACT

Recently, the CNC/GEL (cellulose nanocrystals/gelatin) composite hydrogel has been used as a biomaterial for 3D printing of tissue engineering scaffolds. Rheological properties of hydrogel have been regarded as one of the most important factors affecting printing quality, especially the viscosity recover time. However, there is still a lack of comprehensive research on the rheology property of the CNC/GEL hydrogel in the process of 3D printing. In this study, the CNC was isolated from *Humulus japonicus*, and a CNC/GEL hydrogel system was prepared. The rheological properties of CNC/GEL hydrogel were evaluated using a rotary rheometer. The viscosity recovery time of the CNC/GEL hydrogel was measured using a special method. The optimal ratio of hydrogel was obtained by rheology experiment and mechanical test. The flow field distribution of the hydrogel in the flow passage of 3D printer was analyzed using fluent simulation. The rheological parameters of a hydrogel can be adjusted by changing the printing conditions. Thus, the effect of printing conditions on the formation of CNC/GEL filaments was also investigated. Finally, the biocompatibility of the printed CNC/GEL scaffold after crosslinking treatment was verified using CCK-8 and Hoechst 33342/PI double-staining assays. The present study shows a new approach for the analysis of rheological properties of CNC/GEL and also provides some suggestions for 3D printing of CNC/GEL scaffolds.

Handling Editor: Jaime Grunlan.

Address correspondence to E-mail: jpzhou@yzu.edu.cn

https://doi.org/10.1007/s10853-020-05128-x

Introduction

Organ defects caused by trauma or disease lead to great pain and inconvenience in patients [1]. However, traditional organ transplantation is limited by the shortage of donors [2]. The development of tissue engineering provides a new method for organ repair. Tissue engineering scaffolds are a key factor for successful tissue repair. Tissue engineering scaffolds should have biocompatibility and mechanical strength [3]. In addition, tissue engineering scaffolds should also have a three-dimensional porous structure and pore penetration to allow for the transport of nutrients, exchange of oxygen and discharge of waste [4].

As a hydrogel, gelatin (GEL) extracted from animal skin and bones is a good material for 3D bioprinting in tissue engineering because of its good biocompatibility, biodegradability and easy formation [5]. However, simple gelatin has low mechanical strength and fast degradation in the human body, which seriously limits its application [6, 7].

In recent years, cellulose nanocrystals (CNCs) extracted from plants have been widely favored by researchers because of their high strength, high crystallinity and good biocompatibility [8]. CNCs are widely used in tissue engineering as a type of reinforcement material [9–11]. It has been reported that the addition of CNC increased the strength of PVA, sodium alginate, chitosan and collagen scaffolds [12–14]. Pei et al. [15] have reported that the CNC could significantly improve the strength and reduce the swelling of CNC/GEL film. Recently, the CNC/GEL hydrogel has been used as a material for 3D printing [16, 17]. As is well known, the quality and the formation of a scaffold are affected by the rheological properties of the material used for printing [18]. However, there are few researches on the comprehensive evaluation of the rheological behavior of the CNC/GEL hydrogel and its 3D printing process.

Theoretically, an ideal printing material should have thixotropic property and a fast viscosity recovery ability [19]. Hydrogels are non-Newtonian fluids, and the "shear thinning" is a characteristic of non-Newtonian fluids [20, 21]. In the process of 3D printing, the hydrogel is stored in the barrel of 3D printer in advance. Under the air pressure in the barrel, the hydrogel viscosity drops rapidly, resulting in a phenomenon of "shear thinning," which is conducive to the flow of the hydrogel in the barrel and nozzle [18]. Then, when the hydrogel is squeezed out of the nozzle and the shear stress is dissipated, most of the viscosity can be recovered in a short time, and this is conducive to the formation and mechanical strength of the printed construct [22]. Therefore, it is very important to evaluate the rheological properties of the CNC/GEL hydrogels for 3D printing. In particular, determination of the hydrogel viscosity recovery time is one of the key factors to improve the printing quality. If the viscosity of the first printed layer has not recovered, its structure is unstable and its corresponding mechanical strength is relatively low. Then, if the second layer is stacked on the first layer, the printed scaffold is prone to collapse [19]. Thus, the viscosity recover time is a basis for setting the interval time between two adjacent layers in the process of 3D printing. However, it is difficult for us to directly measure it.

What is more, in the process of 3D printing, when the fluid passes through the flow passage, there are frictions between the different fluid layers and resulting in shear stress [23]. Due to the existence of frictions, the flow velocity in the different position of the flow passage is not consistent. Therefore, the flow field distributions in the flow passage are complex. However, there is no instrument that can directly measure the flow characteristics of the fluid in the passage, which makes it inconvenient for us to understand and study the process of 3D printing. Finite element analysis is a method which simulates the real physical system by using mathematical approximation. It can analyze some parameters such as velocity and stress which cannot be measured directly. Thus, the finite element analysis provides a new way for us to solve that problem. In addition, in the process of 3D printing, the rheological parameters of the fluids can be adjusted by changing printing parameters [24]. Murphy et al. [22] have concluded that the nozzle diameter, printing pressure, printing temperature and nozzle moving speed had important influences on the formation of a scaffold. Therefore, in order to improve the printing quality of CNC/GEL scaffold, we need to systematically and comprehensively study its rheological characteristics of CNC/GEL hydrogel, including viscosity recovery time, the flow field distribution in the passage of 3D printer and the effect of varying the rheological characteristics (by adjusting printing parameters) on the forming.

In this study, we isolated CNC from *Humulus japonicus* stem (HJS) and prepared a CNC/GEL hydrogel system. We thoroughly evaluated the rheological properties of the CNC/GEL hydrogel system and determined the viscosity recovery time of the CNC/GEL hydrogel using a special method. The optimal filling content of CNC for the composite hydrogel was determined by combination of rheological evaluation mechanical test. The distributions of shear stress and the shear rate of the CNC/GEL hydrogel in the passage were visually displayed using the fluent simulation. The effects of printing parameters on the formation of the CNC/GEL scaffold were investigated, including printing pressure, nozzle diameter, printing temperature and nozzle moving speed. Finally, the biocompatibility of the printed scaffold after crosslinking treatment was verified using CCK-8 and Hoechst 33342/PI double-staining assays.

Materials and methods

Materials

HJSs were harvested from the Jiangsu Province of China. Genipin was purchased from Linchuan Zhixin Biotechnology Co., Ltd. (Fuzhou, Jiangxi). GEL was of bioreagent grade and supplied by Macklin Biochemical Reagent Co., Ltd. (Shanghai, China). Other chemicals were of analytical reagent grade and purchased from Sinopharm Chemical Reagent Co., Ltd. (Shanghai, China).

Preparation of CNC and CNC/GEL

Isolation of CNC from the HJS has been reported in our previous work [28]. Briefly, the HJS powder was treated with 4% NaOH at 80 °C for 2 h and then bleached with $NaClO_2$ at 80 °C for 6 h to obtain purified cellulose. The purified cellulose was hydrolyzed using 60% sulfuric acid at 45° for 1 h with strong agitation. Then, the mixture was centrifuged followed by dialysis (8000-10000D, RC) until its pH was 7 to obtain the CNC suspension.

The GEL was dissolved in phosphate-buffered solution (PBS) at 40°. CNC suspensions were added to the GEL solution in the desired proportion and stirred evenly and then put them in a refrigerator at 4 °C for 2 h until they transformed into gel form sol.

In these prepared hydrogel samples, the GEL content was always 5%, but the CNC content was varied. The selected CNC contents (F_{CNC}) were 0, 5, 10 and 15% ($F_{CNC} = M_{CNC}/(M_{CNC} + M_{GEL}) \times 100\%$), respectively. These samples are, respectively, referred to as GEL-5, 5%-CNC/GEL-5, 10%-CNC/GEL-5 and 15%-CNF/GEL-5.

Shear rate in an extrusion-based 3D printing process

In the process of 3D printing, the CNC/GEL hydrogel material is assumed to move at a speed of v along the axis of the barrel and nozzle, and the axial direction is the Z coordinates. Hydrogel is a non-Newtonian fluid, and the power law is usually used to describe its flow characteristics as follows:

$$\eta = K(\dot{\gamma})^{n-1} \tag{1}$$

The constants of n and k can be obtained from the experimental data by curve fitting, and r is the shear rate.

In the 3D printing process, the hydrogel is stored in a barrel with a circular cross section and moves to the nozzle in response to pressure. Usually, the hydrogel shows a steady laminar flow because of its high viscosity. Assuming that the radius of the circular section of the barrel is R, there is a micro-cylinder with a radius of r in the axial direction and with a length of L. The shear stress on the surface of the cylinder is τ, and the pressure on the two end faces of the cylinder is P and $P + \Delta P$, as shown in Fig. 1a. Driven by the pressure gradient (p/L), the micro-cylinder moves forward. After the fluid reaches a steady laminar flow state, the driving force acting on the micro-cylinder unit and the resistance existing in the adjacent liquid layer are in equilibrium. The forces on the two ends are shown in formula (2):

$$p(\pi r^2) = (p + \Delta p)\pi r^2 + 2\tau\pi rL \tag{2}$$

According to formula (2), the distribution of shear stress can be obtained as shown in formula (3):

$$\tau = \frac{\Delta p}{2L} r \tag{3}$$

It can be seen from formula (3) that under the action of a pressure gradient (p/L), the shear stress τ is directly proportional to its distance to the axis (r). It reaches a maximum ($\tau_R = \Delta p \times R/2L$) at the wall and zero at the center. The distribution of shear stress is

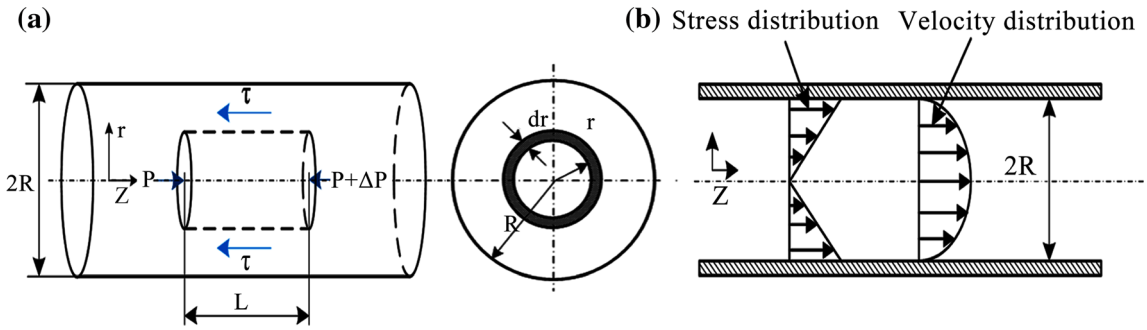

Figure 1 **a** The diagram of fluid flow forces in a circular pipe [25], **b** fluid stress and velocity distribution in a circular pipe [23].

shown in Fig. 1b. Assuming that the flow velocity (V) in the pipeline is uniform, the volume flow velocity (Q) of a non-Newtonian fluid can be expressed as shown in Eq. (4):

$$Q = \pi R^2 V = \pi\left(\frac{n}{3n+1}\right)\left(\frac{-\Delta p}{2mL}\right)^{\frac{1}{n}} R^{\left(\frac{3n+1}{n}\right)} \tag{4}$$

The shear rate ($\dot{\gamma}$) of the fluid in the pipeline can be expressed as formula (5):

$$\dot{\gamma} = r\left[\frac{VR^2}{\left(\frac{n}{3n+1}\right)R^{\left(\frac{3n+1}{n}\right)}}\right] \tag{5}$$

Assuming that the volume of the hydrogel does not change before and after printing, the ratio of the fluid shear rate in the barrel to that in the nozzle can be expressed as formula (6):

$$\frac{\dot{\gamma}_2}{\dot{\gamma}_1} = \left(\frac{D_1}{D_2}\right)^{\left(3+\frac{1}{n}\right)} \tag{6}$$

D_1 and D_2 represent the inner diameter of the barrel and nozzle, respectively.

Finite element simulation of the printing process

The barrel and nozzle photograph are shown in Fig. 2a–c, and their specific sizes are shown in Table 1.

We utilized CERO in FLUENT software to mesh the barrel and the nozzle model, adopting a tetrahedral mesh model, and set the inlet and outlet of the fluid domain, as shown in Fig. 2d, e. The viscosity (η) and flow index (k) of the sample were obtained from the rheological measurement results by curve fitting, and the density of the sample was obtained through measurement (the detailed data are shown in Table S1 in the supplementary materials), and the results are shown in Table 2. By substituting these parameters in the formula: $R_e = \rho UL/\mu$, we could calculate that the R_e (Reynolds number) was less than 2000. Therefore, the laminar model was used in this process. We kept the barrel and nozzle still, applied a uniform load at the inlet (0.1 MPa) of the barrel, and 0 MPa at the outlet of the nozzle. We set the boundary conditions and specified the iteration algorithm.

3D printing test

GEL-5, 5%-CNC/GEL-5, 10%-CNC/GEL-5 and 15%-CNC/GEL-5 hydrogel were used for printing.

(1) Viscosity recovery test. We printed a circle and observed the filament width and height at 0, 15, 30, 45 and 60 s after finishing the printing. We printed a two-layer scaffold and observed the filament width at 1, 10, 20, 30 and 60 min after finishing the printing. (2) We printed a single filament at a pressure of 0.05, 0.06, 0.07, 0.08, 0.09, 0.10, and 0.11 MPa with the same other parameters. (3) We printed a single filament with a nozzle moving speed of 10, 15, 20, 25 and 30 mm/s with the same other parameters. (4) We printed a single filament at a temperature of 5, 15, 20 and 25 °C with the same other parameters. (5) We printed a single filament using a nozzle with a diameter of 210, 280 and 410 μm.

Characterization

Rheological evaluations of hydrogels

The rheological characterizations of all of the hydrogel samples were investigated using a Discovery Hybrid Rheometer-3 (TA instruments, USA). (1) Dynamic strain scan test: at a fixed frequency, we

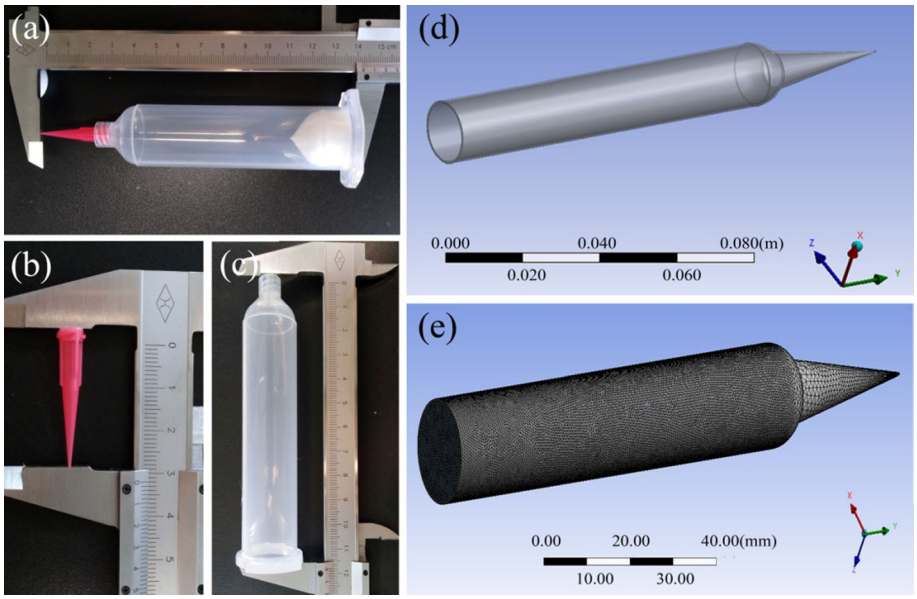

Figure 2 The dimensions of the sprayer (**a**), nozzle (**b**), and barrel (**c**), **d** three-dimensional structural model of the barrel and sprinkler, **e** mesh division of the barrel and sprinkler.

Table 1 Dimensions of barrel and nozzle

Diameter of barrel (mm)	Length of barrel (mm)	Length of nozzle (mm)	Diameter of nozzle (mm)
15.71	96.04	32	0.21

Table 2 Material parameters of 10%-CNC/GEL-5 at 15°

Material	Viscosity (Pa.s)	Flow index (1)	Density (kg m^{-3})
10%-CNC/GEL-5	25.55	0.30	1.002

applied a strain scan from 0.1 to 100% to determine the linear viscoelastic range. (2) Dynamic frequency scanning test: we kept the strain constant at 1% and applied a frequency scan from 0.1 to 100 rad s^{-1}. (3) Steady-state shear rate tests were performed at 5 °C, 10 °C, 15 °C, 20 °C and 25 °C, and the shear rate ranged from 0.01 to 100 s^{-1}. (4) Keeping the shear rate at 20 s^{-1}, the viscosities of the samples were measured in two ways: continuous measurement and intermittent measurement at different time points and finally (5) viscosity recovery test and (6) phase transition temperature ($T_{sol–gel}$) test.

Mechanical property measurements

The solution samples were poured into a PTFE mold (as shown in Fig. 6a) and then put them in a refrigerator at 4° for 2 h until they transformed into gel form sol.

A universal tensile testing machine (HLD-0824, Handpi Co., Ltd., China) was used to measure the hydrogel mechanical strength via a uniaxial compression test method. The elastic modulus hydrogel samples were obtained by the ratio of stress and strain within a linear deformation range. The hydrogel samples were cylindrical and had diameter of 15 ± 1 mm and height of 10 ± 1 mm. The tests were performed at a compression speed of 0.5 mm s^{-1} at 15°. The process of this experiment is shown in Fig. 6a.

Morphological features of the samples

The printed filament and scaffold were observed using a digital camera (S2900HD, FinePix Co, Ltd., Japan). The filament width was measured with a digital image processing program (Image J, National Institutes of Health, USA).

The assays for verification of the biocompatibility

First, we added a certain amount of genipin to tri-distilled water and stirred the mixture until it was completely dissolved. A genipin solution with a concentration of 0.1 M was obtained. Then, the freshly printed 10%-CNC/GEL-5 scaffold was put into the genipin solution and was left to stand at 10 °C for 24 h. Finally, a sufficiently crosslinked scaffold could be obtained, named G-10%-CNC/GEL-5 scaffold.

Extraction of the maceration solution The crosslinked 10%-CNC/GEL-5 scaffold was sterilized with ethylene oxide and then immersed in the culture medium [(89 vol% Dulbecco's modified Eagle's medium (DMEM), 10 vol% fetal bovine serum (FBS) and 1 vol% penicillin/streptomycin)] for 24 h. Finally, we took out the scaffold and collected the leaching liquor after centrifugation.

Cell growth inhibition This experiment was divided into two groups. 3T3 cells (1.0×10^3 cells/well) were seeded in 96-well plates with the leaching liquor (test group) or culture medium (control group) (100 μL/well) and incubated in a CO_2 incubator at 37 °C. Then, the CCK-8 reagent (Beyotime Institute of Biotechnology, Shanghai, China) was added to the plates (10 μL/well) at 1, 3, 5 and 7 days. The cells were then incubated for 2 h. Finally, the absorption at 450 nm was measured for each well using an automatic microplate reader (Thermo Scientific, Shanghai, China) to determine the number of proliferating cells.

Cell apoptosis rate This experiment was divided into two groups. The cells were incubated with the leaching liquor (test group) or with culture medium (control group) in 24-well plates. At the 48-h point, the 3T3 cells were stained with Hoechst 33,342 (10 ng/mL^{-1}) and PI (10 ng/mL^{-1}) (Beyotime Institute of Biotechnology, Shanghai, China) at 4 °C in the dark for 20 min. Then, the condensed or fragmented nuclei of the apoptotic cells were observed using fluorescence microscopy.

Morphological differences The 3T3 cells were seeded in G-10%-CNC/GEL-5 hydrogel and cultured for 48 h. Then, the sample was washed with PBS, fixed with 2.5% glutaraldehyde, washed with PBS, dehydrated with an ethanol gradient (50, 70, 80, 90, 100%) and dried with a critical-point dryer. Finally, a field emission scanning electron microscope (S-4800, Hitachi Co., Ltd., Japan) was used to observe the morphology of the 3T3 cells in the hydrogel after sputtering with gold.

Statistical analysis

Data are expressed as the mean of at least three replicates ± standard deviation (SD). The results were analyzed for variance. Least significant difference multiple comparison tests were used to determine the significant differences between the mean values. Significant differences between two groups were determined using two-tailed Student's t-tests. A confidence level of 95% ($P < 0.05$) was used, and the analyses were performed using SPSS software version 17.0 (SPSS, Inc., Chicago, USA).

Results and discussion

Rheological Evaluation

Effect of shear rate and temperature on viscosity For understanding the printability of CNC/GEL hydrogels, it is important to know their rheological properties. In this experiment, the effect of shear rate on viscosity was studied and the results are shown in Fig. 3a. It can be observed that the viscosity of all samples decreased with the increasing shear rate, proving that all of the samples had the characteristics of "shear thinning." That was due to the disentanglement of the polymer networks in the hydrogel in response to the action of the shear stress. When the disentanglement rate was greater than the network reconstruction rate, the hydrogels would appear to be thinning, along with a decrease in viscosity.

This characteristic is very important since it is conducive to the flow of the hydrogel in the barrel and nozzle of a 3D printer. In addition, it can be observed that the influence of CNC content on the viscosity of the composite hydrogels decreased with the increasing shear rate. That was probably because when the shear rate reached a certain value, the disentanglement rate of intermolecular weak bonds in the hydrogel reached an equilibrium value [23]. Furthermore, the viscosity of the CNC/GEL composite hydrogels was higher than the pure GEL-5. The viscosity of the composite hydrogels increased with the increasing CNC content, up to a maximum for the 10%-CNC/GEL-5. However, when the CNC content was higher than 10%, the viscosity of the

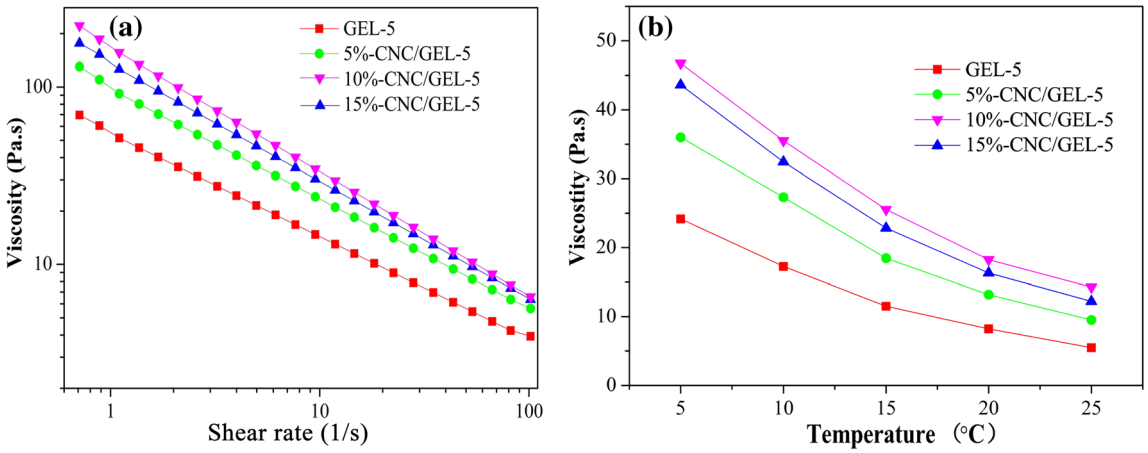

Figure 3 **a** Viscosity as a function of shear rate for different samples at room temperature, **b** viscosity of different samples at different temperatures.

composite hydrogel decreased. It is speculated that CNC agglomeration occurred in the hydrogel system when the CNC content was higher than 10%. The SEM images of hydrogel samples confirmed this speculation (as shown in Fig. S1 in supplementary material).

Steady-state rheological tests were performed at 5°, 10°, 15°, 20° and 25°. Then, the viscosities (η) and the flow indexes (k) of the sample at different temperatures were obtained by curve fitting according to formula (1). (The detailed data are shown in Table S1 in the supplementary materials.) The viscosity–temperature curves of all of the hydrogel samples are shown in Fig. 3b. It can be observed that the viscosity of all samples decreased with increasing temperature. Most likely, the higher temperature accelerated the rate of macromolecular motion, which made it more difficult to form weak bonds among the macromolecules, thereby leading to a decrease in hydrogel viscosity [24]. In addition, the viscosities of the other composite hydrogels were all higher than the pure GEL-5. This was because the addition of CNC improved the total solids content in the composite hydrogel, and the density of the network structure, which resulted in a higher viscosity.

Effect of time on viscosity In Fig. 3a, we can observed that the viscosity of the composite hydrogel sample decreased when the CNC content was higher than 10%. We speculated this result was due to the occurrence of CNC agglomeration in the composite hydrogel. However, if the hydrogel samples are kept for a period of time, will the CNC agglomeration become more serious and the viscosities of hydrogels change? To solve this problem, we further investigated the effect of time on the viscosities of the composite hydrogels. It can be observed from Fig. 4a, b that the viscosities of all the samples changed little in the periods of 0–30 min and 0.5–12 h. We think that the CNC/GEL hydrogel viscosities could not be disturbed by the time. As is well known, a hydrogel material was of different form but similar to a solid material, and the internal structure of the hydrogel is network and porous [21]. In the CNC/GEL hydrogel, the pore wall was composed of GEL and CNC, and water as a medium was captured in the pores. Usually, ions can move freely in a hydrogel by osmosis [26]. The CNC is made of thousands of glucose molecules which linked into giant chains [8]. Probably, it is difficult for CNC to move freely in a hydrogel because its huge volume caused a massive resistance. In addition, due to the existence of molecular interactions between the CNC and GEL, the molecules' thermal motion of CNC could only occur in a small space. The CNC could not move freely and continue to form more agglomerations in the CNC/GEL hydrogel; therefore, the viscosity of CNC/GEL hydrogel has no time-varying characteristic.

The viscosity recovery of hydrogels To study the viscosity recovery after extrusion from the nozzle of the 3D printer, this experiment was divided into three steps: (1) We applied a shear rate of 0.1 s^{-1} and maintained it for 60 s. (2) We increased the shear rate to 100 s^{-1} at 60 s and maintained it for 10 s to mimic the hydrogel flow in the nozzle of the 3D printer. (3) We reduced the shear rate to 0.1 s^{-1} at 70 s and

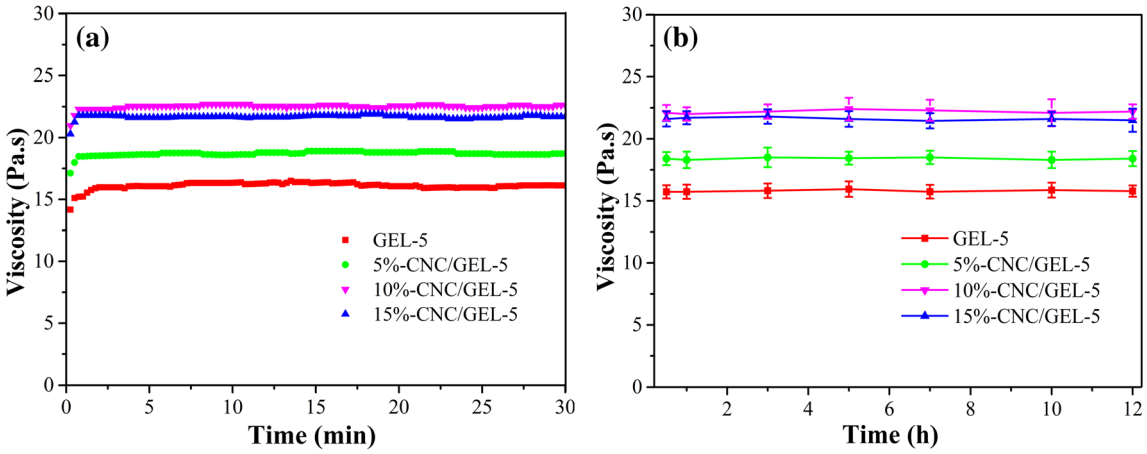

Figure 4 **a** The viscosity variations of hydrogel samples in the period of 1–30 min, **b** the viscosities of hydrogel samples at different time points.

maintained it for 60 s to mimic the hydrogel after being extruded. The results are shown in Fig. 5a.

For 10%-CNC/GEL-5, its viscosity was 838.18 Pa.s in the first stage, and it dropped to 6.66 Pa.s in the second stage and then rose to 718.24 Pa.s at 100 s (30 s after the shear stress was dissipated) in the third stage, which was 85.69% of that in the first stage. The viscosity recovery rates of 15%-CNC/GEL-5, 5%-CNC/GEL-5 and GEL-5 were, respectively, 81.26%, 80.37% and 74.42% at 30 s after the shear stress was dissipated. From 100 to 130 s, the viscosity of all of the hydrogel samples changed slowly. This was

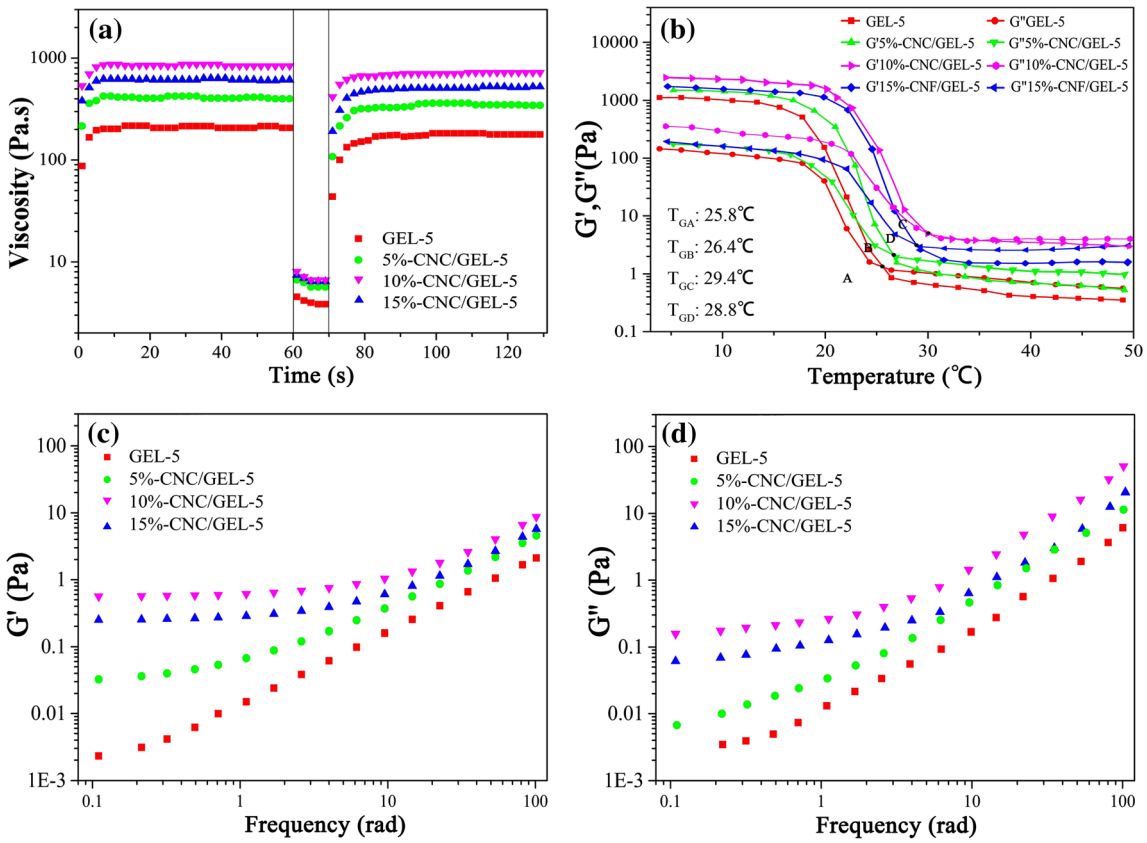

Figure 5 **a** The recovery behavior of different samples with increasing temperature, **b** change in the storage modulus (G') and loss modulus (G'') for all of the samples, the variation of G' (**c**) and G'' (**d**) with increasing frequency.

probably because the shear stress destroyed the physical bonds existing among the macromolecules in the hydrogels, and the reconstruction of the bond needed a longer time [27].

The phase transition temperature ($T_{sol–gel}$) and viscoelasticity of hydrogel The modulus–temperature curves of the hydrogel samples are shown in Fig. 5b. When the temperature increased, the G' (storage modulus) and the G'' (loss modulus) all conversely decreased, and the G' decreased more rapidly than the G''. If the $G' > G''$, the system exhibits a solid-like material, and if $G' < G''$, the system exhibits a liquid-like material. The $T_{sol–gel}$ of GEL-5,5%-CNC/GEL-5, 10%-CNC/GEL-5 and 15%-CNC/GEL-5 was 26.4, 29.4 and 28.8°, respectively. This indicated that the addition of CNC increased the $T_{sol–gel}$ of the composite hydrogel. This was due to the formation of intermolecular hydrogen bonds among hydroxyl, amino and carboxyl groups in the CNC and GEL. These hydrogen bonds hindered the molecules' thermal motion, thus slowing down the disentanglement construction rate of the network structure [28, 29].

Furthermore, we further investigated the viscoelastic behavior of the hydrogel. The dynamic elastic modulus (G') and viscosity modulus (G'') of all of the hydrogel samples at different frequencies are shown in Figs. 5c and 4d. It can be observed that the G' and G" depended on the angular frequency (ω) for all samples. In addition, the CNC was beneficial to improve the G' for the composite hydrogels. However, the G' of 15%-CNC/GEL-5 was lower than that of 10%-CNC/GEL-5. This was probably due to the agglomeration of CNC in 15%-CNC/GEL-5, which was not conducive to stress transfer, thereby leading to a decrease in the elastic modulus.

The results of mechanical test

As shown in Fig. 6a, when a 20 g weight was placed on the top of the GEL-5 and 10%-CNC/GEL-5 hydrogels, GEL-5 completely collapsed, whereas the 10%-CNC/GEL-5 hydrogel remained intact. This indicated that the mechanical strength of the 10%-CNC/GEL-5 was much higher than that of GEL-5. It can be observed from Fig. 6b, c, the breaking strengths and the elastic modulus of the composite hydrogel samples increased with the increasing CNC content when the CNC content was no more than 10%. At the point of 10%, the breaking strength and the elastic modulus of the 10%-CNC/GEL-5, respectively, reached maximums of 365037.59 Pa and 41015.46 Pa, which was 5 times and 8.9 times of the GEL-5. When the CNC content was higher than 10%, the breaking strength and elastic modulus decreased. This phenomenon was consistent with the conclusion which was concluded by storage modulus evaluation in rheology experiment as shown in Fig. 5c, d. This was probably because that a high CNC content caused CNC agglomerations, which resulted in many defects and inhomogeneity in the hydrogel. Thus, the mechanical properties of hydrogel decreased.

In addition, we further investigated the effect of time on the mechanical strength hydrogels, and the results are shown in Fig. 6d. It can be observed that the breaking strength and elastic modulus of 10%-CNC/GEL-5 hydrogel all changed little during the retention period ranging from 0 to 12 h. This result suggested that the mechanical properties of the hydrogels were not disturbed by the retention periods. Probably, that was because the CNC had no fluidity in the CNC/GEL hydrogel which had a structure similar to solid material. The structure of the hydrogel was in a relatively stable state if there was no external force interference.

The results of finite element simulation

Although the distribution of shear stress and velocity field can be obtained by theoretical derivation, it is difficult to directly observe or measure them during the actual process of 3D printing. Therefore, we used ANSYS software to simulate the 3D printing process of 10%-CNC/GEL-5 hydrogel in this part.

The distribution of flow velocity We applied a pressure of 0.1 MPa at the inlet of the fluid, analyzed the points on the reference line and obtained the distribution of the flow rate as shown in Fig. 7a. It can be seen that the closer to the inner wall of the passage, the lower the fluid flow velocity, and the maximum flow velocity was in the central axis of the passage. These simulation results are consistent with the conclusion derived from the theoretical model (as shown in Fig. 1b). That was because there was friction between adjacent layers in the 10%-CNC/GEL-5 hydrogel due to its high viscosity. The highest friction is in the inner wall of the passage, while the lowest friction is located in the center of the passage, resulting in the highest flow velocity in the center of the passage.

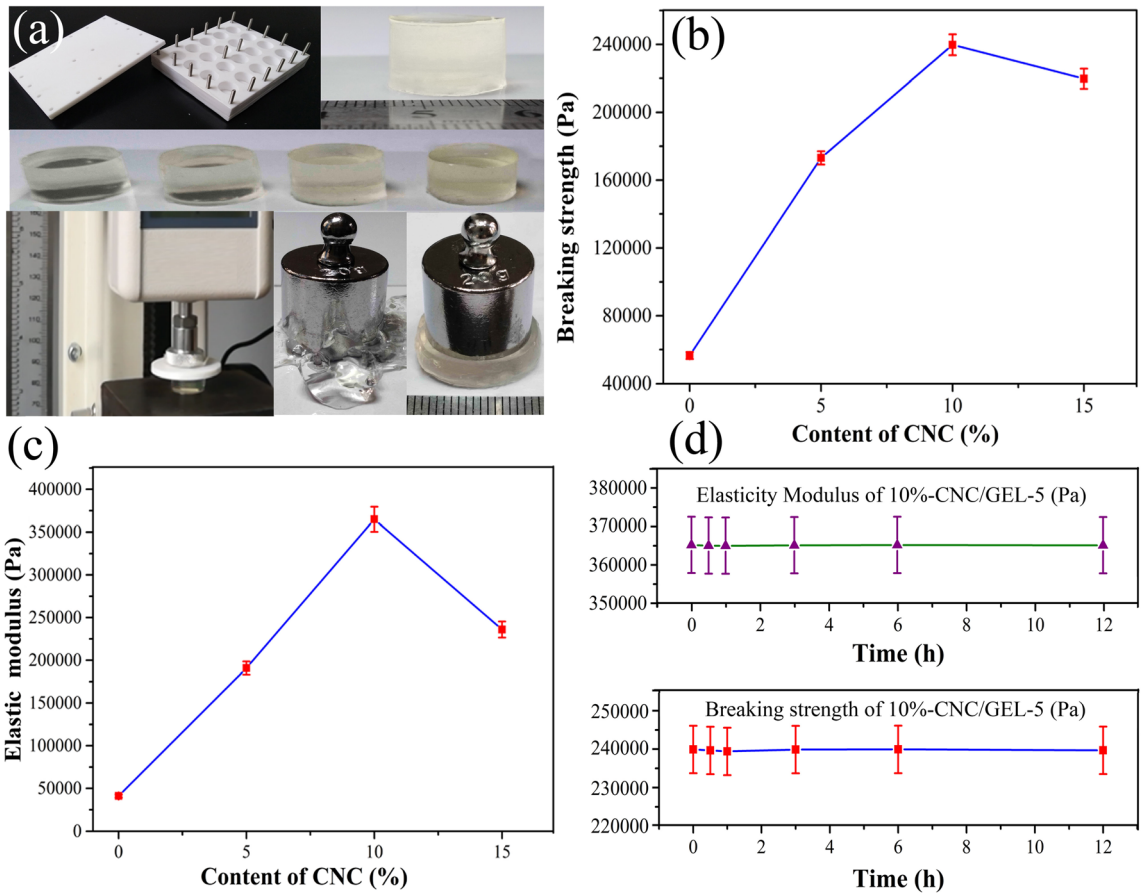

Figure 6 **a** The process of mechanical properties test and mechanical strength comparison of GEL-5 with 10%-CNC/GEL-5, **b** the breaking strength and **c** the elasticity modulus of hydrogel samples with different CNC content, **d** the variation of breaking strength and the elasticity modulus with the increasing storing time.

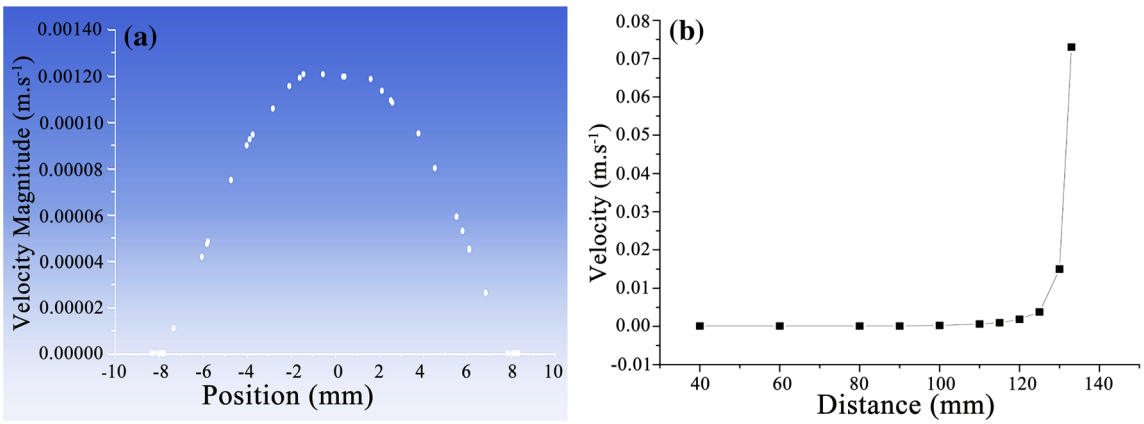

Figure 7 **a** Velocity profile along the diameter direction in the inner section of the barrel, **b** the change of velocity in the whole flow channel with the distance.

To further study the changes of flow velocity in the longitudinal direction of the passage, we arbitrarily selected 11 reference lines parallel to the cross section of the passage, and the distances between the reference lines and the entrance of the barrel ranged from 40 to 133 mm. The flow rates at the midpoint of the 11 reference lines are shown in Fig. 7b. The velocity changed slowly when the distance was less

than 120 mm, and increased rapidly when the distance exceeded 120 mm. This indicated that the flow velocity varied little in the barrel but rapidly in the nozzle. This was due to a rapid reduction in the cross section of the flow passage from the cylinder to the nozzle.

The distribution of shear stress Based on the point analysis of the reference lines, the shear stress distribution was obtained, as shown in Fig. 8a. It can be seen that the shear stress reached a minimum at the center of the passage, while it reached a maximum near the inner wall of the passage. This was because the adjacent layers of the fluid slid with each other, resulting in a reduction in friction in the adjacent layers. Thus, the friction existing in the inner wall was the highest. The shear stress at the midpoint of the 11 reference lines is shown in Fig. 8b. The shear stress changed slowly at first and then rapidly when the distance exceeded 120 mm. This was due to the rapid reduction of the cross section of the passage from the cylinder to the nozzle.

The change of the hydrogel volume We simulated the shape of the hydrogel before and after extrusion from the nozzle, and the results are shown in Fig. 9a. It can be seen that the volume of the hydrogel expanded after extrusion from the nozzle. This was because that hydrogel is a viscoelastic material [30]. When the hydrogel flowed in the passage, it was extruded and decreased in volume. After the hydrogel was extruded out of the nozzle, the extrusion pressure disappeared and the volume of the hydrogel recovered, accompanied by a certain degree of expansion.

3D printing of hydrogel

The phenomenon of extrusion swelling As shown in Fig. 9b, the diameter of the extruded hydrogel was significantly larger than that of the nozzle. This phenomenon was consistent with the results of the finite element simulation. This was because when the hydrogel flowed into the nozzle from the barrel, the hydrogel was subjected to an intense tensile and underwent elastic deformation due to the sharp variation of the passage. The energy, generated in the process of elastic deformation, was stored in the hydrogel. After the hydrogel outflowed from the nozzle, the stored elastic potential energy in the hydrogel was transformed into elastic deformation. This process of energy release was accompanied by the phenomenon of extrusion swelling of the hydrogel sample.

The effect of viscosity recovery on formation The rheological test results showed that most of the hydrogel viscosity could be recovered at 30 s after the shear stress was dissipated (as shown in Fig. 5a). In this experiment, the effect of this viscosity recovery on the formation of printed filaments was studied. Figure 10a shows the photographs of the filaments at 0–60 s after printing. Figure 10b, c, respectively, shows the variation of the filament width and height. It could be observed that the filament width and height of all of the samples decreased rapidly at 0–30 s and then slowly at 31–60 s. This was because the shear stress disappeared as soon as the printing was finished, and then, the physical bonds destroyed by the shear stress in the hydrogel rebuilt rapidly, leading to a volume shrink along with a rise in the

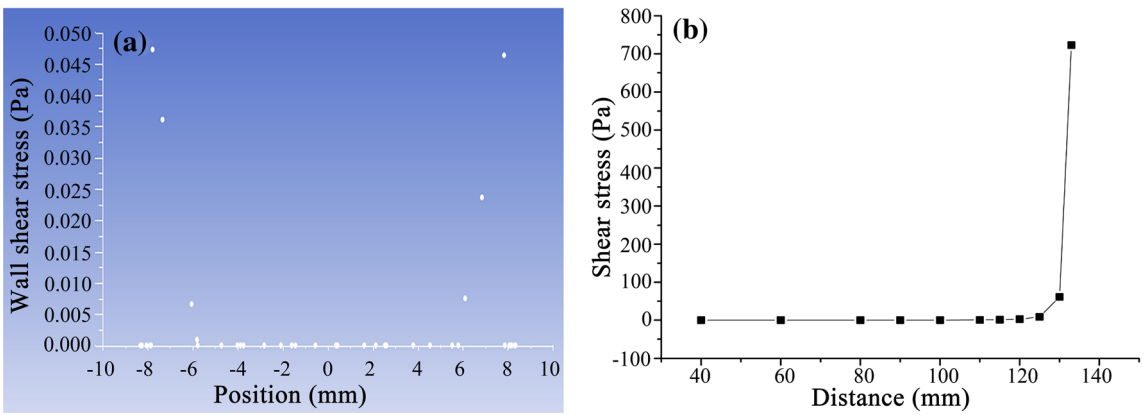

Figure 8 **a** Shear stress distribution along the diameter direction in the inner section of the barrel, **b** diagram of the variation of shear stress with distance.

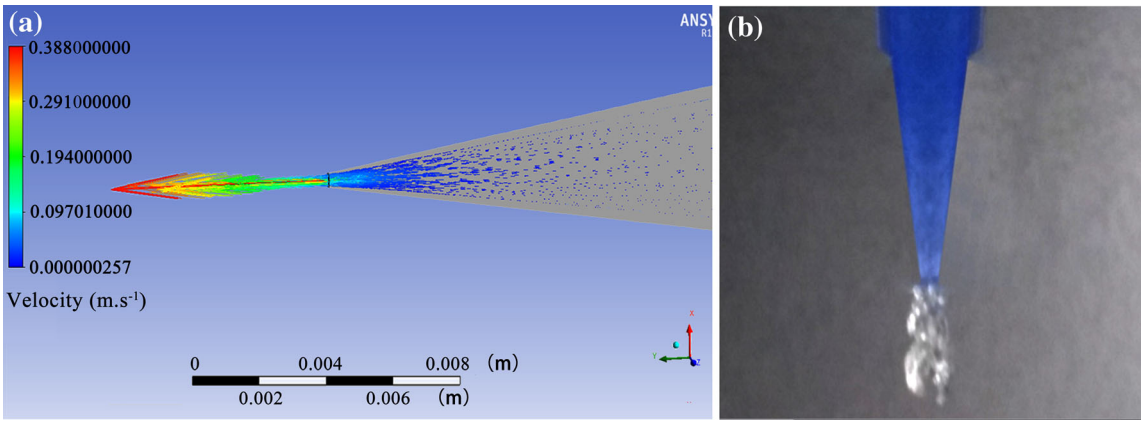

Figure 9 **a** Expansion of the extrusion part after the nozzle, **b** the extrusion swelling phenomenon.

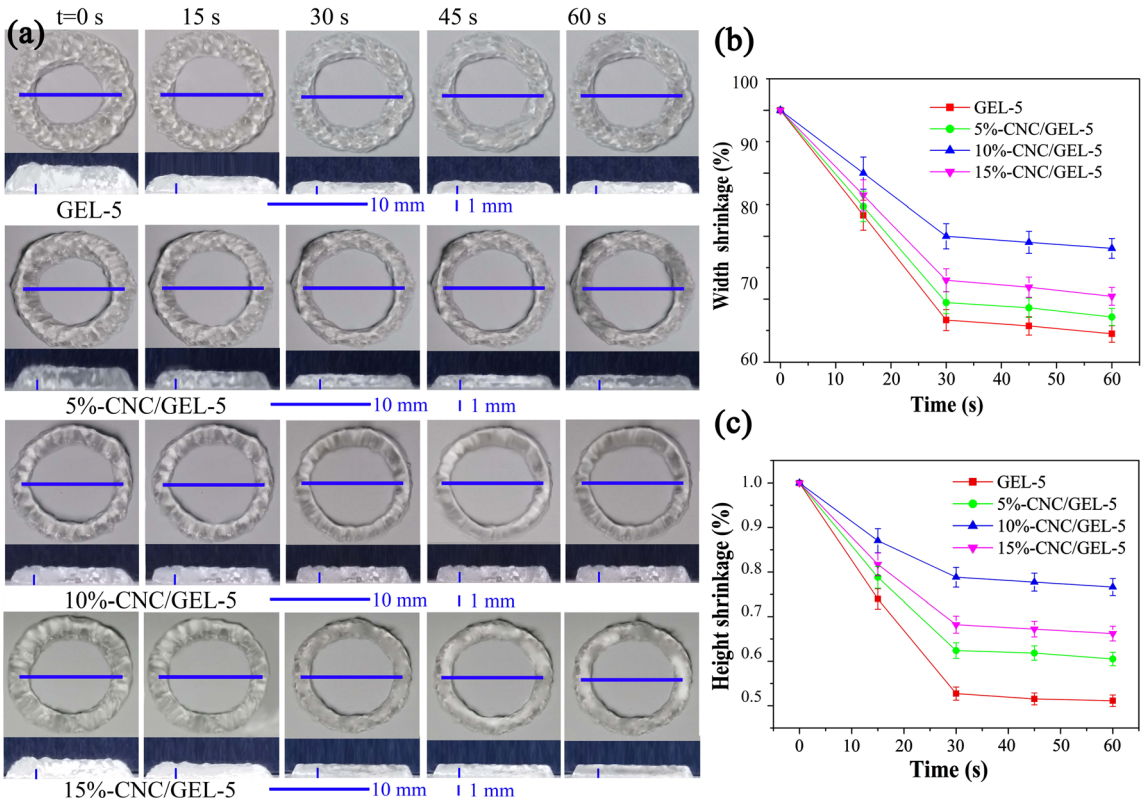

Figure 10 **a** The photographs of the printed different hydrogels at the different recovery times, the width shrinkage (**b**) and the height shrinkage (**c**) with time after printing.

hydrogel viscosity [32]. In addition, it can be observed that the 10%-CNC/GEL-5 had the smallest shrinkage rate in width and height. This confirmed the findings of the rheological test that the viscosity of 10%-CNC/GEL-5 was higher than the other samples. Furthermore, we further studied the morphology of the 10%-CNC/GEL scaffold at 1–60 min after printing. The results are shown in Fig. 11a, b. The change of filament width of the printed scaffold morphology and filament width were very small during 1–60 min. These results indicated that the filament shrinkage mainly occurred within 30 s after printing, and then, the scaffold reached a balance and maintained its morphology. This filament shrinkage time was the same as the hydrogel viscosity time.

In fact, a scaffold is usually composed of multilayers, and the shrinkage rate and shrinkage period of each layer should be fully considered. The results

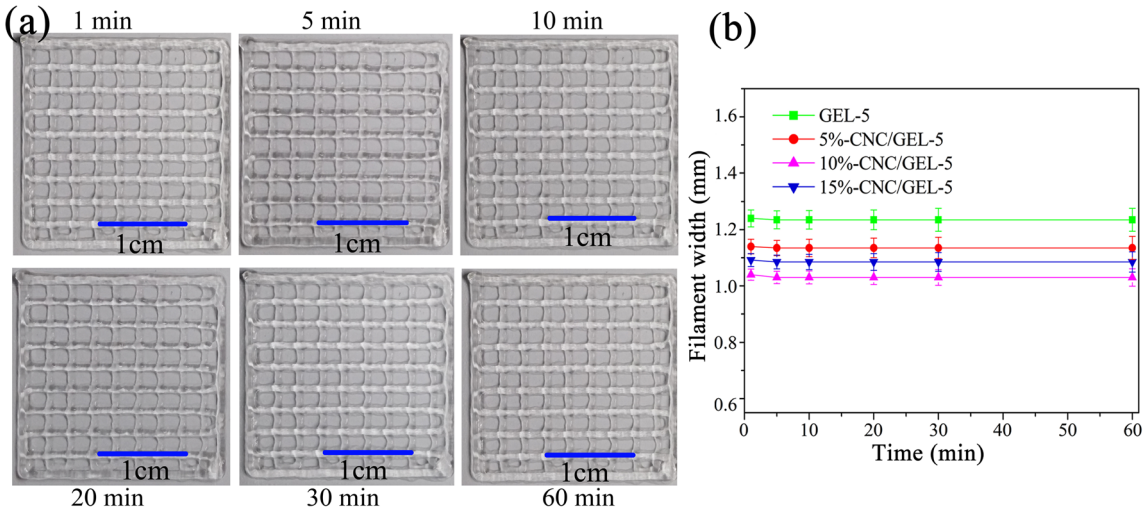

Figure 11 **a** The photographs of the printed 10%-CNC/GEL-5 hydrogel scaffold at different aging times, **b** the widths of all the filaments at different aging times.

in this experiment provide a reference for setting the layer height and printing time of each layer in the 3D printing process.

The effect of printing pressure and temperature on formation The widths of the filaments printed under different pressures are shown in Fig. 12a. (The photographs are shown in Fig. S2 in the supplementary materials.) It can be seen that the filament widths of all of the samples increased almost linearly with the increasing pressure. This result was caused by several reasons: (1) Increasing pressure caused more fluid flow and more volume of hydrogel to be extruded from the nozzle per unit time; (2) the higher pressure resulted in a larger hydrogel deformation in the passage and a higher extrusion swelling rate of the printed filament; (3) the higher pressure led to a higher stress and more obvious shear thinning of the hydrogels, which lead to a higher extrusion swelling rate of the printed filaments [31].

Figure 12b shows the filament width at different printing temperatures. (The photographs are shown in Fig. S3 in the supplementary materials.) It can be observed that the filament widths of all of the samples increased with the increasing printing temperature. According to Arrhenius theory: $\eta = Ae^{\Delta E_\eta/RT}$, if the temperature rose, the macromolecules in the hydrogel could move more quickly and the

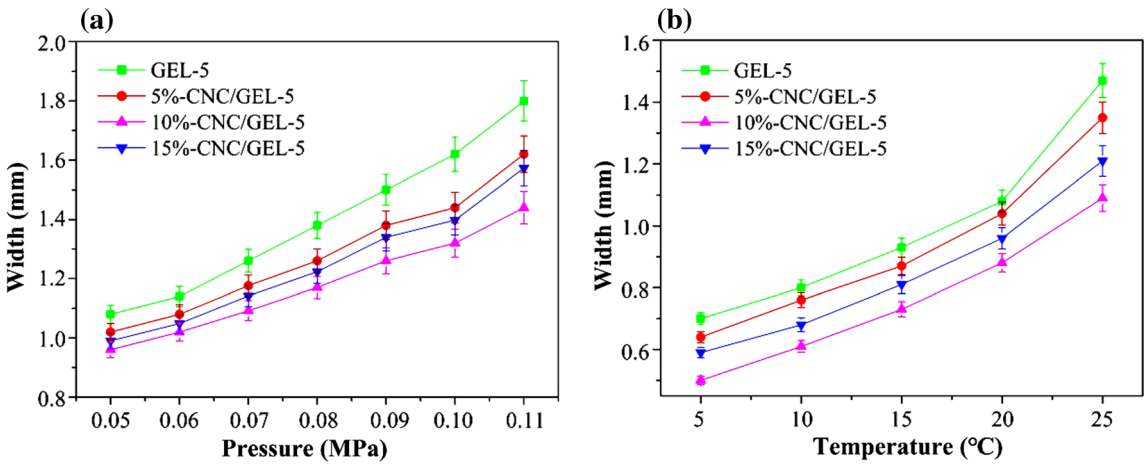

Figure 12 **a** The variation curves of filament width with the increasing pressure, **b** the variation curves of filament width with the printing temperature.

intermolecular forces became weaker [33]. This lead to a decrease in the hydrogel viscosity and an increase in filament width [32]. This conclusion is consistent with the rheological test results. In addition, it was observed that there were width turning points for all of the filament samples at 20 °C. This was because when the temperature was near to the $T_{sol-gel}$ of the hydrogels (as shown in Fig. 5b), the viscosities of the hydrogels decreased sharply.

The effect of nozzle diameter and nozzle moving speed on the formation effect The widths of the printed filaments using nozzles with different diameters (0.21, 0.26 and 0.41 mm) are shown in Fig. 13a. (The photographs are shown in Fig. S4 in the supplementary materials.) It can be observed that the widths of all of the filament samples increased with the increasing nozzle diameter. This was because a lager diameter of the nozzle had a more serious damping effect and less effective pressure. The decrease in effective pressure reduced the extrusion amount of the hydrogel and caused a decrease in the shear stress, which maintained the hydrogel viscosity at a higher value [34]. Thus, the filament width decreased.

Figure 13b shows the widths of filaments printed at different nozzle moving speeds (10, 15, 20 and 25 mm/s). (The photographs are shown in Fig. S5 in the supplementary materials.) It can be seen that the width of all of the filament samples decreased with the increasing nozzle moving speed. This is because the faster the nozzle moved, the lower the amount of hydrogel extruded on the receiving platform per unit time, leading to a decrease in filament width.

The results of cell viability and proliferation

Cell growth inhibition The CCK-8 assay was used to evaluate cell growth inhibition of the G-10%-CNF/GEL-5 hydrogel as a scaffold material, and the result is shown in Fig. 14a ($p < 0.05$). It can be seen that the optical density (OD) values increased with the increasing culture time, and the differences in the OD values between the test and control group were very small. This finding indicated that the growth and proliferation of 3T3 cells was supported by the leaching liquor of the G-10%-CNC/GEL-5 scaffold.

Morphological differences The SEM images of 3T3 cells growing on the G-10%-CNF/GEL-5 hydrogel coating are shown in Fig. 14b. It can be seen there were multiple layers of cells in the hydrogel, and the cells exhibited a spindle shape and pseudopod extensions, indicating that these cells grew well. These results suggested that the G-10%-CNF/GEL-5 hydrogel (the photograph of the G-10%-CNF/GEL-5 scaffold is shown in Figure S6 in the supplementary materials) could support cell growth and provide channels for cell migration and proliferation.

Cell apoptosis rate Live/dead cell staining was performed to assess the induction of apoptosis by the G-10%-CNF/GEL-5 scaffold. The live cells stained blue are shown in Fig. 14$c^{0'}$, $c^{1'}$, and the dead cells stained red are shown in Fig. 13$c^{0''}$, $c^{1''}$. The merged images of the live and dead cells are shown in Fig. 14c^{0}, c^{1}. Evidently, there were many live 3T3 cells and few dead cells in both the test and control groups. The cell apoptosis rates for the test and

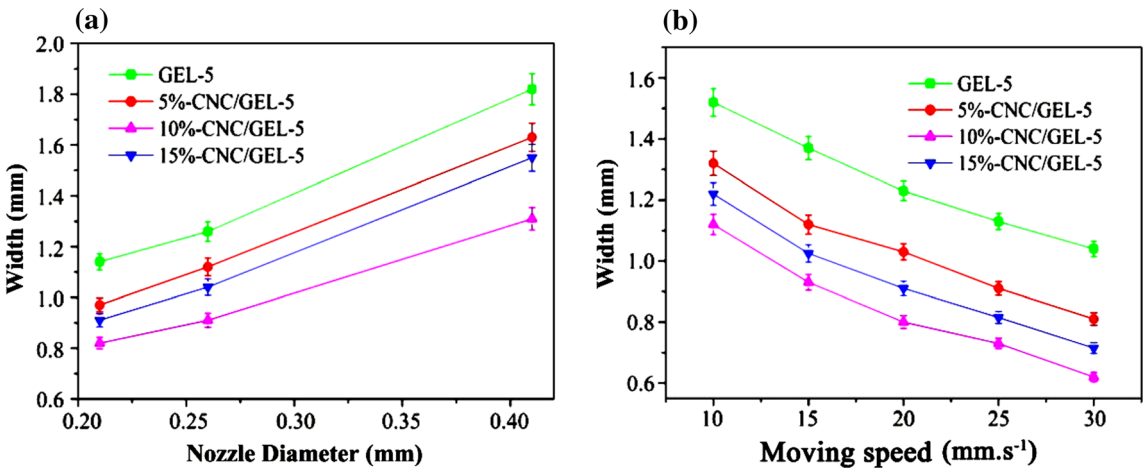

Figure 13 **a** The variation curves of filament width with the nozzle diameter, **b** the variation curves of filament width with the nozzle moving speed.

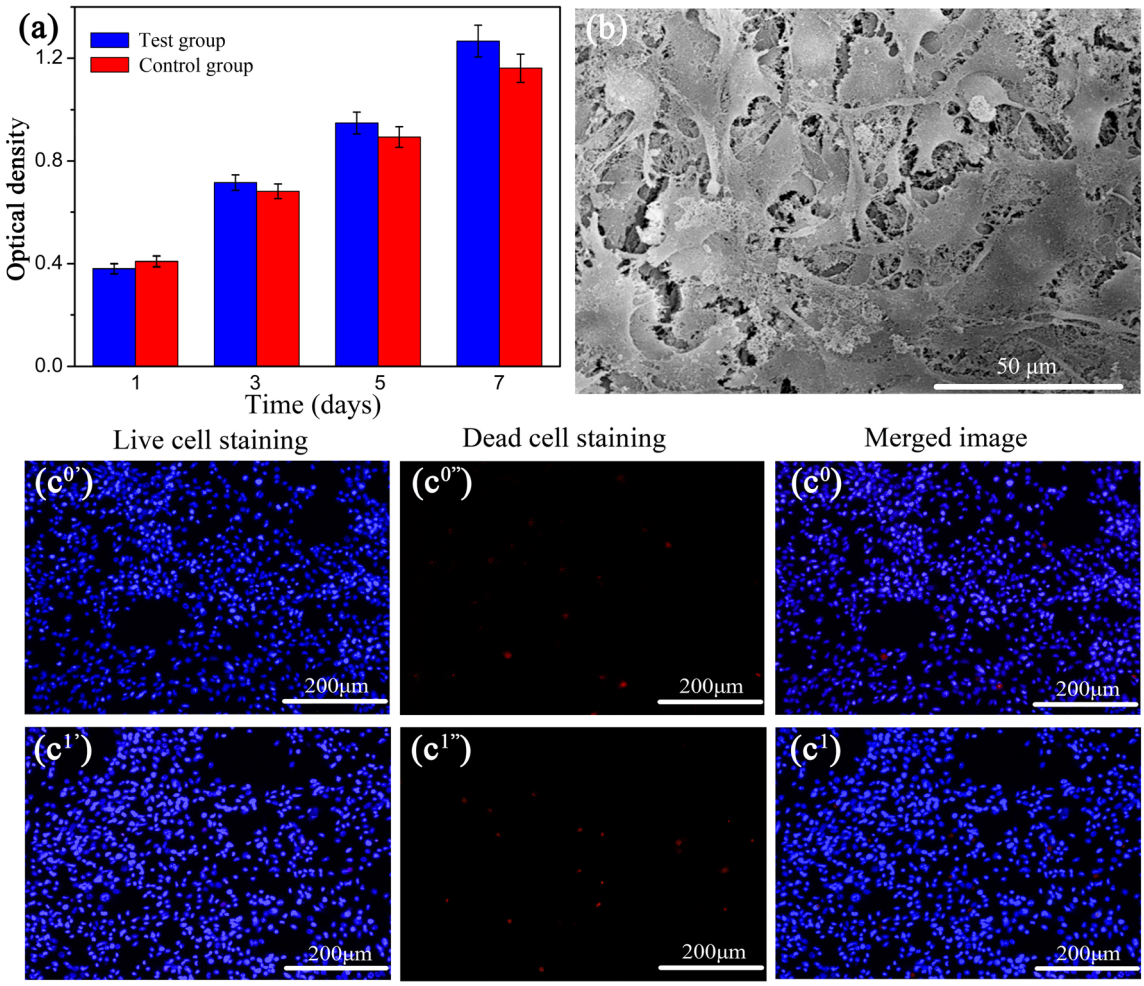

Figure 14 **a** The variation trend of the optical density (OD) of 3T3 cells with the increasing culture days, **b** the SEM image of 3T3 growing on G-10%-CNF/GEL-5 hydrogel, **c** the fluorescence photographs of 3T3 cells of test ($\mathbf{c^{1'}}$, $\mathbf{c^{1''}}$, $\mathbf{c^{1}}$) and control groups ($\mathbf{c^{0'}}$, $\mathbf{c^{0''}}$, $\mathbf{c^{0}}$) after culture for 48 h.

control groups were 1.29 ± 0.04% ($p < 0.05$) and 1.05 ± 0.03% ($p < 0.05$), respectively. There were only minor differences in cell apoptosis rates between the test and control groups, suggesting that the G-10%-CNF/GEL-5 scaffold does not obviously induce apoptosis.

Conclusions

In this paper, we isolated CNC from HJS and prepared a CNC/GEL hydrogel system. The thixotropic property and viscosity recovery time of the CNC/GEL hydrogels were proven to be important for printing, and the recovery time for the CNC/GEL hydrogel was confirmed to be approximately 30 s. The result of rheological experiment and mechanical test all showed that when the content of CNC was 10%, the mechanical strength of the 10%-CNC/GEL was up to a maximum. The results of FLUENT simulation suggested that the shear stress reached a minimum at the center of the position and a maximum near the inner wall of the passage, while the closer to the inner wall of the passage, the smaller the fluid flow velocity, and the maximum flow velocity was in the central axis of the flow passage. Furthermore, by comparing the width of the printed filament, we found that adjusting the rheological parameters of the CNC/GEL hydrogel by changing the printing conditions, including the printing pressure, nozzle diameter, printing temperature, nozzle moving speed, could improve the printing quality. The results of cell viability and proliferation assay confirmed the biocompatibility of the CNC/GEL

scaffolds after crosslinking treatment. These results concluded in this paper study can give a new approach for the analysis of rheological properties of hydrogels and also provide some suggestions for 3D printing of CNC/GEL scaffolds.

Acknowledgements

This research was supported by the Natural Science Foundation of China (51775483), the Natural Science Foundation of Yangzhou (YZ201976), the Natural Science Foundation of China (81770018), the Top Talents Support Program of Yangzhou University.

Electronic supplementary material: The online version of this article (https://doi.org/10.1007/s10853-020-05128-x) contains supplementary material, which is available to authorized users.

References

[1] Subramanian A, Albert V, Mishra B, Sanoria S, Pandey RM (2016) Association between the pancreatic enzyme level and organ failure in trauma patients. Trauma Mon 21(2):e20773

[2] Park K, Lee JH, Huh KH, Kim SI, Kim YS (2004) Diminution of donor organ shortage. Transplantat Proc 36(10):2949–2951

[3] Li WJ, Tuli R, Okafor C, Derfoul A, Danielson KG, Hall DJ, Tuan RS (2005) A three-dimensional nanofibrous scaffold for cartilage tissue engineering using human mesenchymal stem cells. Biomaterials 26:599–609

[4] Tai H, Mather ML, Howard D, Wang W (2007) Control of pore size and structure of tissue engineering scaffolds produced by supercritical fluid processing. Eur Cells Mater 14(1):64–77

[5] Jiang Y, Zhou J, Yang Z, Liu D, Xv X, Zhao G, Shi H, Zhang Q (2018) Dialdehyde cellulose nanocrystal/gelatin hydrogel optimized for 3D printing applications. J Mater Sci 53:11883–11900. https://doi.org/10.1007/s10853-018-2407-0

[6] Li M, Guo Y, Wei Y, MacDiarmid AG, Lelkes PI (2016) Electrospinning polyaniline-contained gelatin nanofibers for tissue engineering applications. Biomaterials 27:2705–2715

[7] Xing Q, Yates K, Vogt C, Qian Z, Frost MC, Zhao F (2015) Increasing mechanical strength of gelatin hydrogels by divalent metal ion removal. Scientific Reports 4:1–10

[8] Sadeghifar H, Filpponen I, Clarke SP, Brougham DF, Argyropoulos DS (2011) Production of cellulose nanocrystals using hydrobromic acid and click reactions on their surface. J Mater Sci 46:7344–7355. https://doi.org/10.1007/s10853-011-5696-0

[9] Bačáková L, Novotná K, Pařízek M (2014) Polysaccharides as cell carriers for tissue engineering: the use of cellulose in vascular wall reconstruction. Physiol Res 63(1):29–47

[10] Yu H, Sun B, Zhang D, Chen G, Yang X, Yao J (2014) Reinforcement of biodegradable poly (3-hydroxybutyrate-co-3-hydroxyvalerate) with cellulose nanocrystal/silver nanohybrids as bifunctional nanofillers. J Mater Chem B2(48):8479–8489

[11] Nicharat A, Shirole A, Foster EJ, Weder C (2017) Thermally activated shape memory behavior of melt-mixed polyurethane/cellulose nanocrystal composites. J Appl Polym Sci 134(27):45033

[12] Benavides EE, Brown PJ, Kitchens CL (2010) Effect of jet stretch and particle load on cellulose nanocrystal/alginate nanocomposite fibers. Langmuir 26(17):14263–14270

[13] Ureña-Benavides EE, Brown PJ, Kitchens CL (2010) Effect of jet stretch and particle load on cellulose nanocrystal-alginate nanocomposite fibers. Langmuir ACS J Sur Colloids 26(17):14263–14270

[14] Yang W, Zheng Y, Chen J, Zhu Q, Feng L, Lan Y, Zhu P, Tang S, Guo R (2019) Preparation and characterization of the collagen/cellulose nanocrystals/USPIO scaffolds loaded kartogenin for cartilage regeneration. Mater Sci Eng 99:1362–1373

[15] Pei Y, Xv G, Li Y, Zheng X, Liu J, Tang K (2017) Fabrication, structure and properties of cellulose nanowhiskers/gelatin composite film. Polym Mater Sci Eng 033(008):45–49

[16] Rastin H, Ormsby RT, Atkins GJ, Losic D (2020) 3D bioprinting of methylcellulose/gelatin-methacryloyl (MC/GelMA) bioink with high shape integrity. ACS Appl Bio Mater 3:1815–1826

[17] Yan H, Chen X, Feng M, Shi Z, Zhang D, Lin Q et al (2017) Layer-by-layer assembly of 3D alginate-chitosan-gelatin composite scaffold incorporating bacterial cellulose nanocrystals for bone tissue engineering. Mater Lett 29:492–496

[18] Smith PT, Basu A, Saha A, Nelson A (2018) Chemical modification and printability of shear-thinning hydrogel inks for direct-write 3D printing. Polymer 152:42–50

[19] Chen Y, Wang YH, Yang Q (2018) A novel thixotropic magnesium phosphate-based bioink with excellent printability for application in 3D printing. J Mater Chem B 6(27):4502–4513

[20] Ding HZ, Chang RC (2018) Printability study of bioprinted tubular structures using liquid hydrogel precursors in a support bath. Appl Sci 8(3):403

[21] Pei X (2013) Comparison of rheologic properties between Ca-alginate hydrogel microspheres suspension and whole blood. J Biomed Eng 30(1):100–104

[22] Panda B, Ruan S, Unluer C, Tan MJ (2019) Improving the 3D printability of high volume fly ash mixtures via the use of nano attapulgite clay. Composites 165:75–83

[23] Habib A, Sathish V, Mallik S, Khoda B (2018) 3D printability of alginate-carboxymethyl cellulose hydrogel. Materials 11(3):454

[24] Murphy SV, Atala A (2014) 3D bioprinting of tissues and organs. Nat Biotechnol 32(8):773–785

[25] Gu L (2017) Research of hydrogel and cell printing technique for skin tissue engineering. Doctoral dissertation, Zhejiang A&F University

[26] Makino K, Suzuki K, Sakurai Y, Ohshima Teruo Okano Hiroyuki (1995) Electro-osmosis on a thermosensitive-hydrogel surface. J Colloid Interface Sci 174(2):400–404

[27] Yang Y, Xie X, Yang Z, Wang X, Cui W, Yang J (2007) Controlled synthesis and novel solution rheology of hyperbranched poly (urea-urethane)-functionalized multiwalled carbon nanotubes. Macromolecules 40(16):5858–5867

[28] Lian C (2014) Forming mechanism and mechanical properties of the strong nanocomposite hydrogels. Master dissertation, South China University of Technology

[29] Xiong YL, Blanchard SP (1994) Dynamic gelling properties of myofibrillar protein from skeletal muscles of different chicken Parts. J Agric Food Chem 42(3):670–674

[30] Liu KL, Zhang Z, Li J (2011) Supramolecular hydrogels based on cyclodextrin–polymer polypseudorotaxanes: materials design and hydrogel properties. Soft Matter 7(24):11290–11297

[31] Liang Q, Zhang S, Zhang J (2012) Rheological behaviors and microstructure of Oviductus Ranae hydrogels. Food Sci Biotechnol 21(2):467–474

[32] Jiang Z, Cao X, Li Z, Guo L (2016) Rheological behaviors and secondary networks of polyacrylamide hydrogel filled with silica. J Pet Explor Prod Technol 6(1):93–99

[33] Limbach HH, Lopez JM, Kohen A (2006) Arrhenius curves of hydrogen transfers: tunnel effects, isotope effects and effects of pre-equilibria. Philos Trans R Soc Lond Ser B Biol Sci 361(1472):1399–1415

[34] Hu J, Wang L, Shi R, Xu M (2017) The state-of-the-art of 3D bio-printing of skin tissues. Sci Sin (Vitae) 47(4):423–442